

Worm-like emulsion droplets

Jatin Abacousnac, Wenjun Chen, Jasna Brujic, and David G. Grier
*Department of Physics and Center for Soft Matter Research,
 New York University, New York, NY 10003, USA*

Forming an interface between immiscible fluids incurs a free-energy cost that usually favors minimizing the interfacial area. An emulsion droplet of fixed volume therefore tends to form a sphere, and pairs of droplets tend to coalesce. Surfactant molecules adsorbed to the droplets' surfaces stabilize emulsions by providing a kinetic barrier to coalescence. Here, we show that the bound surfactants' osmotic pressure also competes with the droplet's intrinsic surface tension and can reverse the sign of the overall surface free energy. The onset of negative surface tension favors maximizing surface area and therefore favors elongation into a worm-like morphology. Analyzing this system in the Gibbs grand canonical ensemble reveals a phase transition between spherical and worm-like emulsions that is governed by the chemical potential of surfactant molecules in solution. Predictions based on this model agree with the observed behavior of an experimental model system composed of lipid-stabilized silicone oil droplets in an aqueous surfactant solution.

The droplets in oil-in-water emulsions generally minimize their interfacial area to lower their free energy. This mechanism favors the formation of spherical droplets and promotes droplet coalescence. Droplets can be kinetically stabilized against coalescence by binding surfactant molecules to the oil-water interface. Here, we describe an additional dramatic consequence of surfactant binding, illustrated in Fig. 1, in which the osmotic pressure of bound molecules drives a spherical emulsion droplet through a phase transition to a worm-like morphology. Worm-like emulsions are distinct from worm-like micelles [1, 2] because they are stabilized by surfactant concentrations far below the critical micelle concentration (CMC). They also differ from the varied morphologies of liposomes and vesicles, which are dictated by the bending and curvature moduli of surfactant bilayers [3]. The sphere-to-worm transition in suitable emulsions constitutes an alternative pathway for morphology control in soft matter.

Our study of worm-like emulsions is inspired by the observed behavior of micrometer-scale droplets of a ternary oil mixture stabilized by lipid surfactants and dispersed in water [4]. This model system has been studied extensively as a building block of emulsion-droplet chains known as colloidomers [5]. Individual droplets ordinarily form spheres, as shown in Fig. 1(a). We find that adding a cosurfactant, such as sodium dodecyl sulfate (SDS), can cause these droplets to elongate into flexible worm-like structures such as the example in Fig. 1(b). Spherical droplets are observed to deform continuously into worms when their dispersion is cooled a few degrees, and reform into spheres upon heating. The transformation is reversible through repeated cycles. Simple linear worms result from quasistationary cooling and more complex morphologies emerge at higher cooling rates.

The observed phenomenology of worm-like emulsions is captured by the minimal model depicted schematically in Fig. 2. This model treats an oil droplet as the substrate for a two-dimensional classical gas of surfactant

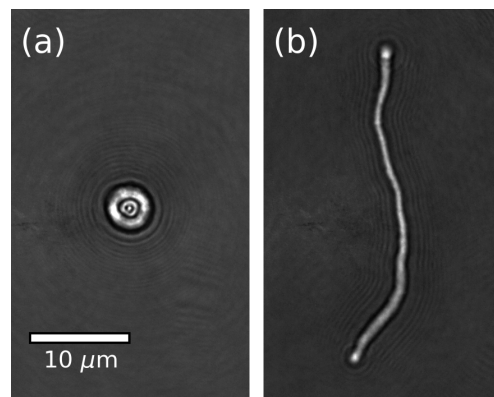


FIG. 1. Holographic images of a lipid-stabilized emulsion droplet composed of a ternary oil mixture, dispersed in an aqueous SDS solution at 1 mM: (a) in the spherical morphology at $(23 \pm 1)^\circ\text{C}$ and (b) in the flexible worm-like morphology at a slightly lower temperature, $(21 \pm 1)^\circ\text{C}$.

molecules. Each surfactant molecule has mass m and subtends an area Ω on the droplet's surface. Surfactant molecules bind to the surface with a binding energy, ϵ , that we assume to be independent of coverage. A system of N bound molecules therefore has the Hamiltonian

$$H_N = \sum_{n=1}^N \frac{p_n^2}{2m} - N\epsilon, \quad (1)$$

where \mathbf{p}_n is the two-dimensional momentum of the n -th molecule on the droplet's surface. The associated canonical partition function is

$$\begin{aligned} Z(A, T, N) &= \frac{1}{N!} \frac{1}{h^{2N}} \int e^{-\beta H_N} \prod_{j=1}^N d^2 r_j d^2 p_j \quad (2a) \\ &= \frac{1}{N!} \frac{1}{A_Q^N} \left(A - \frac{1}{2} N \Omega \right)^N e^{N\beta\epsilon}, \quad (2b) \end{aligned}$$

where h is Planck's constant, $\beta^{-1} = k_B T$ is the thermal energy scale at absolute temperature T , A is the droplet's

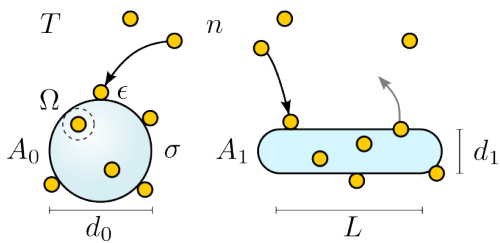


FIG. 2. Schematic representation of surfactant molecules (yellow) binding to a spherical emulsion droplet, thereby inducing it to adopt a worm-like morphology.

surface area, and

$$A_Q(T) = \left[\frac{4\pi}{h^2} \int_0^\infty p \exp\left(-\beta \frac{p^2}{2m}\right) dp \right]^{-1} \quad (3a)$$

$$= \frac{h^2}{2\pi m k_B T} \quad (3b)$$

is the quantum area for the bound molecules. The term in parentheses on the right-hand side of Eq. (2b) is the effective area of the droplet's surface after accounting for the area occupied by surfactant molecules.

Bound surfactant molecules are in thermodynamic equilibrium with the bulk solution of free surfactant molecules at chemical potential μ . In establishing this equilibrium, the osmotic pressure of the molecules on the surface favors increasing the droplet's surface area by deforming the droplet into a noncompact shape such as a worm. Increasing the surface area, however, incurs a cost in surface energy through the fluid's intrinsic surface tension, σ . We account for changes in the droplet's surface area and surfactant coverage with the Gibbs grand canonical partition function,

$$\mathcal{Q}(\sigma, \mu, T) = \int_{A_0}^{A_1} \frac{dA}{A_Q} \sum_{N=0}^{M(A)} \mathcal{Z}(A, T, N) e^{\beta N \mu} e^{-\beta \sigma A}, \quad (4)$$

where $A_0 = \pi d_0^2$ is the surface area of the bare spherical droplet at diameter d_0 , and A_1 is the maximum area of the deformed worm-like droplet. The minimum area is set by the droplet's volume. The maximum area is limited by factors such as the bending energy of the lipid surfactant [1] whose microscopic mechanisms we do not address in the present study. Assuming that surfactant molecules do not overlap, close packing limits the coverage to $N \leq M(A) = A/\Omega$.

Equation (4) can be recast as

$$\mathcal{Q}(\sigma, T, \mu) = \int_{A_0}^{A_1} \frac{dA}{A_Q} \mathcal{Z}(A, T, \mu) e^{-\beta \sigma A}, \quad (5)$$

in terms of the grand canonical partition function,

$$\mathcal{Z}(A, T, \mu) = \sum_{N=0}^{M(A)} \frac{1}{N!} \left(\frac{A - \frac{1}{2} N \Omega}{A_Q} \right)^N e^{\beta N (\epsilon + \mu)}. \quad (6)$$

For simplicity, we assume that the coverage is small enough, $\langle N \rangle \ll A/\Omega$, that we may neglect the excluded area. In this approximation, the grand canonical partition function reduces to

$$\mathcal{Z}(A, T, \mu) \approx \sum_{N=0}^{\infty} \frac{1}{N!} \left[\frac{A}{A_Q} e^{\beta(\epsilon + \mu)} \right]^N \quad (7a)$$

$$= \exp\left(\frac{A}{A_Q} e^{\beta(\epsilon + \mu)} \right). \quad (7b)$$

The Gibbs grand canonical partition function then follows as

$$\mathcal{Q}(\sigma, T, \mu) \approx \int_{x_0}^{x_1} \exp\left(x \left[e^{\beta(\epsilon + \mu)} - \beta \sigma A_Q \right]\right) dx \quad (8a)$$

$$= \frac{e^{-\kappa x_0} - e^{-\kappa x_1}}{\kappa}, \quad (8b)$$

where $x = A/A_Q$ is the dimensionless surface area and

$$\kappa(T) = \beta \sigma A_Q(T) - e^{\beta(\epsilon + \mu)} \quad (9)$$

is a dimensionless parameter that describes the effective surface tension. The sign of $\kappa(T)$ selects the droplet morphology and is determined by the temperature and by the chemical potential of the surfactant molecules.

Treating unbound surfactant molecules as an ideal gas with a bulk number density n , the chemical potential is given by the Sackur-Tetrode formula [7, 8],

$$\mu = k_B T \ln(n V_Q), \quad (10)$$

where $V_Q = A_Q^{\frac{3}{2}}$ is the quantum volume for the molecules in the bulk. Applying this to Eq. (9) suggests that the effective surface tension vanishes along a curve,

$$\frac{n_c(T)}{n_0} = \left(\frac{T_0}{T} \right)^{\frac{1}{2}} \exp\left(-\frac{T_0}{T}\right), \quad (11)$$

that serves as the phase boundary between the spherical and worm-like morphologies. This curve is plotted in Fig. 3(a). The temperature scale in Eq. (11) is set by the surfactant's binding energy through

$$T_0 = \frac{2\epsilon}{k_B}, \quad (12)$$

while the characteristic concentration scale,

$$n_0 = \sqrt{\frac{2\pi m \sigma^2}{h^2 \epsilon}}, \quad (13)$$

balances binding energy against surface tension.

The effective surface tension is positive in the absence of dissolved surfactant molecules, $n = 0$, which is consistent with the expectation that emulsion droplets ordinarily form spheres. Conversely, $\kappa(T)$ is strictly negative when the concentration of dissolved surfactant molecules

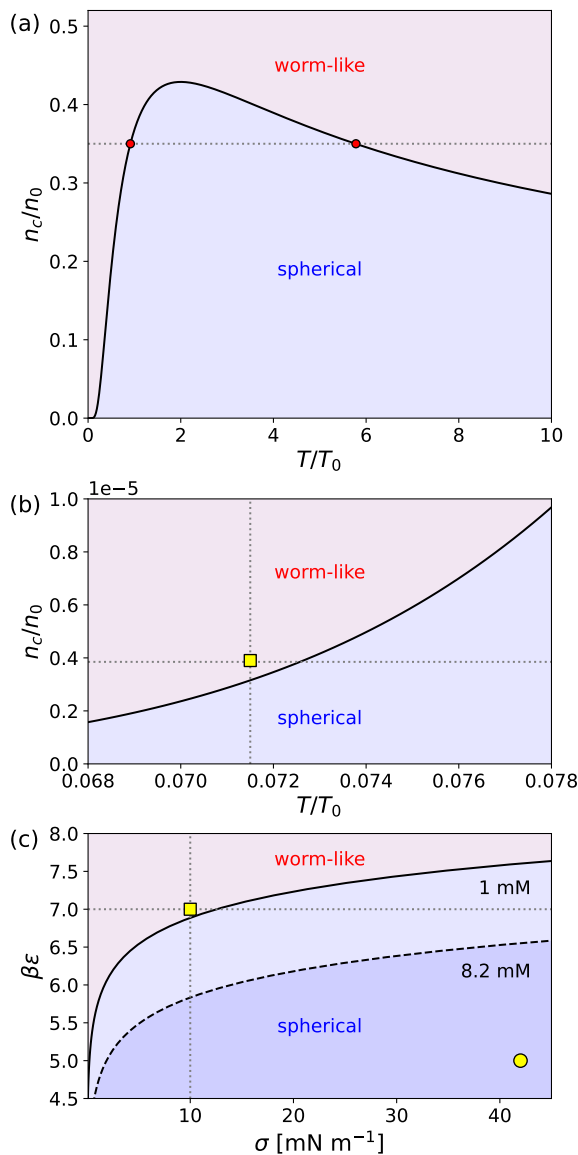


FIG. 3. (a) Phase boundary between spherical and worm-like morphologies predicted by Eq. (11) as a function of temperature, T , and surfactant concentration, n . (b) Region of the phase diagram around the experimental conditions in Fig. 1, which are plotted as a discrete (square) point. Proximity to the predicted phase boundary is consistent with the system's sensitivity to temperature changes. (c) Phase boundary plotted in terms of the intrinsic interfacial energy, σ , of the droplets and the binding energy for SDS, ϵ , in an SDS solution at 1 mM (solid curve) and at the CMC for SDS (dashed curve). Properties for the ternary oil droplets used for this study fall near the phase boundary at 1 mM (square). Properties for standard silicone oil in SDS solution [6] (circle) lie far from the phase boundary, consistent with observation.

exceeds $n^* = n_0/\sqrt{2e} = 0.429 n_0$. Between these two limiting cases, the sign of the effective surface tension depends on the temperature, with spherical droplets being stable in a range, $T_- < T < T_+$, that is set by the

bulk surfactant concentration.

The average surface area adopted by a droplet can be obtained in the Gibbs grand canonical ensemble,

$$\langle A \rangle = -\frac{1}{\beta} \frac{\partial}{\partial \sigma} \ln \mathcal{Q} \quad (14a)$$

$$= \frac{A_Q (\kappa x_0 + 1) e^{-\kappa x_0} - (\kappa x_1 + 1) e^{-\kappa x_1}}{\kappa (e^{-\kappa x_0} - e^{-\kappa x_1})}. \quad (14b)$$

Assuming that $|\kappa| x_1 \gg |\kappa| x_0 \gg 1$, the sign of κ selects either spheres or worms:

$$\langle A \rangle \approx \begin{cases} A_0, & T_- < T < T_+ \Rightarrow \text{spherical} \\ A_1, & \text{otherwise} \Rightarrow \text{worm-like} \end{cases}. \quad (15)$$

The nature of the surfactant-mediated phase transition is clarified by considering the number of surfactant molecules that are bound to the droplet:

$$\langle N \rangle = \frac{1}{\beta} \frac{\partial \ln \mathcal{Q}}{\partial \mu} = \frac{\langle A \rangle}{A_Q} e^{\beta(\epsilon + \mu)}. \quad (16)$$

This corresponds to a fractional surface coverage,

$$\phi \equiv \Omega \frac{\langle N \rangle}{\langle A \rangle} = n \Omega A_Q^{\frac{1}{2}} e^{\beta \epsilon}, \quad (17)$$

that depends strongly on temperature. High surfactant coverage in the low-temperature phase provides the osmotic pressure needed to overcome the droplet's intrinsic surface tension and destabilize the spherical morphology. Equation (17) also can be used to assess whether or not the surfactant's excluded area can be neglected in deriving Eq. (7). Taking the excluded area into account tends to reduce the number of bound surfactant molecules while also tending to increase their surface pressure. These competing effects influence the phase boundary, $n_c(T)$, quantitatively but not qualitatively.

The predicted sphere-to-worm transition can be compared directly to the observed behavior of emulsion droplets. The droplets used in this study are synthesized from a 1:1:1 mixture by volume of three silane monomers: (a) dimethyldiethoxysilane (Sigma-Aldrich), (b) (3,3,3-trifluoropropyl) methylmethoxysilane (Gelest), and (c) 3-glycidoxypropylmethyldiethoxysilane (Gelest). They are formed into micrometer-scale droplets by ammonia-catalyzed hydrolysis followed by condensation, as described in [9, 10]. The droplets are cleaned and dispersed in 1 mM SDS solution to an overall concentration of 1×10^7 droplets/mL before being stabilized by adding DSPE-PEG-SH lipid (Avanti Polar Lipids, MW 2000) at a concentration of $5 \mu\text{g mL}^{-1}$. This procedure yields droplets with an estimated surface coverage of lipids of roughly 50 percent [10]. Lipids bind irreversibly to the oil-water interface and are not observed to form micelles.

The 1 mM concentration of SDS in our model system phenomenologically is close to the point at which spherical droplets deform into worms. The transformation is

not observed in dispersions that lack SDS. Each SDS molecule has a mass of $m = 4.8 \times 10^{-25}$ kg and subtends $\Omega \lesssim 0.5 \text{ nm}^2$ on the oil-water interface [11]. The interfacial tension is measured with a pendant drop tensiometer (attension, Theta Lite) to be $\sigma = 10 \text{ mN m}^{-1}$ in the absence of SDS, which is consistent with values obtained for similar systems in previous studies [12, 13]. The dependence of the surface energy on SDS concentration yields $\epsilon = 7 k_B T$ for the surfactant binding energy [13]. Equation (17) then yields $\phi \lesssim 2 \times 10^{-3}$ for the fractional surface coverage of SDS at room temperature, which is small enough to justify neglecting Ω in the derivation of $\mathcal{Z}(A, T, \mu)$, but still large enough to drive the transition. Figure 3(b) confirms that the model system's properties lie close to the predicted phase boundary.

Figure 3(c) recasts these results in terms of the surface tension and binding energy at the transition point given the molar mass and concentration of the surfactant. This again confirms that the material properties of the model system are close to the predicted transition point in a 1 mM SDS solution at room temperature. Conventional silicone oils, by contrast, have substantially higher surface tension in contact with water and lower affinity for SDS [6], and therefore lie well within the predicted domain of stability for spherical droplets. Such systems cannot be destabilized into worm-like droplets by increasing the surfactant concentration because the CMC for SDS at 8.2 mM establishes an upper bound on the chemical potential of bound molecules at the interface. This may explain why worm-like emulsions have not been reported previously.

We analyze emulsion droplets' behavior using a custom-built instrument that combines conventional bright-field microscopy, in-line holographic microscopy and holographic optical trapping [14]. The microscope uses an oil-immersion objective lens (Nikon S Plan Apo, $100\times$ numerical aperture 1.4) to achieve a system magnification of 48 nm/pixel on the sensor of a CMOS video camera (Flir Flea3 USB3.0). Holographic imaging is performed at a vacuum wavelength of 447 nm (Coherent Cube) and an intensity of 1 mW mm^{-2} . Holographic trapping is performed at 1070 nm (IPG Photonics YLR-10-LP) using a phase-only spatial light modulator (Holo-eye Pluto). The images in Fig. 1 are holograms of the emulsion droplet that can be used to numerically reconstruct the deformed droplet's three-dimensional structure [15] and to track its motion [16].

The ramified structure in Fig. 4(a) is a worm-like emulsion droplet formed from a spherical droplet by cooling the microscope stage 3°C in 1 min. Rather than continuously elongating into a uniaxial worm, this rapidly cooled droplet nucleated seven worm-like extensions. Even though the individual arms are flexible they do not relax into a uniaxial worm resembling Fig 1(b) presumably because surface osmotic pressure tends to keep them all extended. The formation and stability of such star-

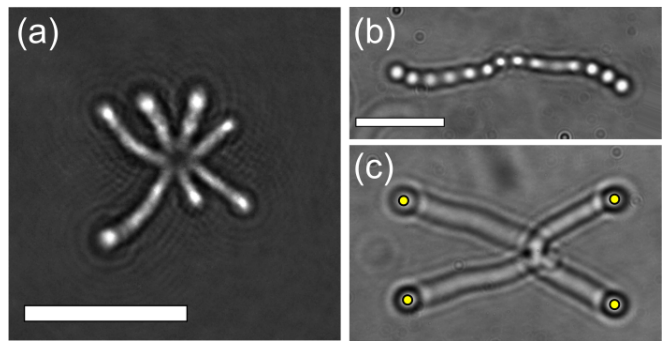


FIG. 4. (a) Holographic image of a multibranching worm-like emulsion formed by rapid cooling (b) Bright-field image of a worm-like emulsion droplet undergoing a pearling instability. (c) Bright-field image of two worm-like emulsion droplets crossed and placed under tension by optical tweezers (yellow circles) projected onto their ends. Scale bars: $10 \mu\text{m}$.

like worms therefore provides additional support for the proposed morphology selection mechanism. Multi-arm droplets contract into spheres upon heating and can be thermally cycled into either uniaxial or ramified worms through the choice of cooling rate.

Rapidly heating a linear worm can induce a pearling instability of the kind depicted in the bright-field image in Fig. 4(b). In this case, the sample's temperature was raised by 3°C over 1 minute, which places it roughly on the predicted phase boundary. The pearling instability does not cause the droplet to break up but does appear to hinder its return to sphericity. The delay may be caused by stress-induced redistribution of lipid surfactants on the droplet's surface, which would require time to relax.

The image in Fig. 4(c) highlights worm-like droplets' stability against coalescence. Two droplets are trapped by holographic optical tweezers that are projected onto their ends. The droplets' axes are made to intersect by moving the traps interactively in three dimensions. The droplets then are placed under an estimated 100 fN of tension by moving the tweezers apart. Each micrometer-diameter trap is powered by 10 mW, and the intense illumination raises the local temperature by roughly 1°C . This localized heating causes the ends of the worms to form spherical bulges that are visible in Fig. 4(c). Despite 2 min of heating and the imposed tension, the two worms do not merge. Extinguishing the optical tweezers allows them to separate and to diffuse independently.

The observations reported in Fig. 4 lend credence to the proposal that the sphere-to-worm transformation is a phase transition and that the worm-like morphology is stabilized by the surface osmotic pressure of bound surfactant molecules. They further demonstrate that the nature of the morphological transformation can be controlled kinetically, with different morphologies appearing at different cooling and heating rates. The discovery of worm-like emulsions in our model system raises the pos-

sibility that similar shape-shifting transformations will be found in other emulsions. The ease with which the sphere-to-worm transformation can be controlled both macroscopically and microscopically suggests that this class of emulsions will be useful for developing active and responsive soft materials [17–20].

We are grateful to Alexander Y. Grosberg, Jacques Fattaccioli, Paul Chaikin, and Aditya Hardikar for helpful conversations. This work was supported by the National Science Foundation through Awards No. DMR-2104837 and DMR-2105255 and the Swiss National Science Foundation through Grant No. 10000141. The integrated instrument for holographic trapping and microscopy was constructed under the MRI program of the NSF through Award No. DMR-0922680.

-
- [1] M. Cates and S. Candau, Statics and dynamics of worm-like surfactant micelles, *J. Phys. Condens. Matter* **2**, 6869 (1990).
- [2] C. A. Dreiss, Wormlike micelles: where do we stand? Recent developments, linear rheology and scattering techniques, *Soft Matter* **3**, 956 (2007).
- [3] A. Zidovska, Membrane shape evolution *in vitro*, in *Handbook of Lipid Membranes*, edited by C. R. Safinya and J. O. Rädler (CRC Press, 2021) Chap. 7, pp. 129–139.
- [4] W. Chen, L. Sixdenier, A. McMullen, D. G. Grier, and J. Brujic, Refractive-index and density-matched emulsions with programmable dna interactions, *Soft Matter* **20**, 4175 (2024).
- [5] A. McMullen, M. Holmes-Cerfon, F. Sciortino, A. Y. Grosberg, and J. Brujic, Freely jointed polymers made of droplets, *Phys. Rev. Lett.* **121**, 138002 (2018).
- [6] A. Kanellopoulos and M. Owen, Adsorption of sodium dodecyl sulphate at the silicone fluid/water interface, *Trans. Faraday Soc.* **67**, 3127 (1971).
- [7] O. Sackur, Die Anwendung der kinetischen Theorie der Gase auf chemische Probleme, *Ann. Phys.* **341**, 958 (1911).
- [8] H. Tetrode, Die chemische Konstante der Gase und das elementare Wirkungsquantum, *Ann. Phys.* **343**, 434 (1912).
- [9] N. A. Elbers, J. Jose, A. Imhof, and A. van Blaaderen, Bulk scale synthesis of monodisperse PDMS droplets above 3 μm and their encapsulation by elastic shells, *Chem. Mater.* **27**, 1709 (2015).
- [10] A. McMullen, M. Muñoz Basagoiti, Z. Zeravcic, and J. Brujic, Self-assembly of emulsion droplets through programmable folding, *Nature* **610**, 502 (2022).
- [11] H. B. de Aguiar, A. G. de Beer, M. L. Strader, and S. Roke, The interfacial tension of nanoscopic oil droplets in water is hardly affected by sds surfactant, *J. Am. Chem. Soc.* **132**, 2122 (2010).
- [12] J. Brujić, S. F. Edwards, D. V. Grinev, I. Hopkinson, D. Brujić, and H. A. Makse, 3D bulk measurements of the force distribution in a compressed emulsion system, *Faraday Discuss.* **123**, 207 (2003).
- [13] J. Lin, I. Jorjadze, L.-L. Pontani, M. Wyart, and J. Brujic, Evidence for marginal stability in emulsions, *Phys. Rev. Lett.* **117**, 208001 (2016).
- [14] M. J. O’Brien and D. G. Grier, Above and beyond: holographic tracking of axial displacements in holographic optical tweezers, *Opt. Express* **27**, 25375 (2019).
- [15] L. Dixon, F. C. Cheong, and D. G. Grier, Holographic deconvolution microscopy for high-resolution particle tracking, *Opt. Express* **19**, 16410 (2011).
- [16] J. Abacousnac, J. Brujic, and D. G. Grier, Measuring colloid hydrodynamics with holographic video microscopy, *Phys. Rev. E* **110**, 014605 (2024).
- [17] J. Tang, P. J. Quinlan, and K. C. Tam, Stimuli-responsive pickering emulsions: recent advances and potential applications, *Soft Matter* **11**, 3512 (2015).
- [18] J. Liu, Y. Gao, Y.-J. Lee, and S. Yang, Responsive and foldable soft materials, *Trends Chem.* **2**, 107 (2020).
- [19] Z. Shen, F. Chen, X. Zhu, K.-T. Yong, and G. Gu, Stimuli-responsive functional materials for soft robotics, *J. Mater. Chem. B* **8**, 8972 (2020).
- [20] I. Apsite, S. Salehi, and L. Ionov, Materials for smart soft actuator systems, *Chem. Rev.* **122**, 1349 (2021).